Research Article | Vol. 31, No. 17 / 14 Aug 2023 / Optics Express 27621
Optics EXPRESS

Probing the decelerating trajectory of a Raman soliton using temporal reflection

JUNCHI ZHANG,[1,*] WILLIAM R. DONALDSON,[2] AND GOVIND P. AGRAWAL[1]

[1]The Institute of Optics, University of Rochester, Rochester, New York 14627, USA
[2]Laboratory for Laser Energetics, University of Rochester, Rochester, New York 14627, USA
[*]jzh156@ur.rochester.edu

Abstract: Temporal reflection is a process where an optical pulse reflects off a moving boundary with different refractive indices across it. In a dispersive medium, this process creates a reflected pulse with a frequency shift that changes its speed. Such frequency shifts depend on the speed of the moving boundary. In this work, we propose and experimentally show that it is possible to probe the trajectory of the boundary by measuring the frequency shifts while changing the initial delay between the incident pulse and the boundary. We demonstrate this effect by reflecting a probe pulse off a short soliton, acting as a moving boundary that decelerates inside a photonic crystal fiber because of intrapulse Raman scattering. We deduce trajectory of the soliton from the measured spectral data for the reflected pulse.

1. Introduction

A significant amount of research has been devoted in recent years to the photonics of time-varying media [1–3]. By actively changing optical properties of a material such as its refractive index, it is possible to realize novel optical phenomena such as large frequency shifts at a temporal discontinuity [4,5], temporal analog of Young's two-slit experiment [6], and amplification of a wave based on momentum band gaps in a photonic time crystal [7,8].

Optical properties of any material can be changed with time through external modulation. One common type of modulation is the so-called spatiotemporal modulation, realized using a traveling wave that creates a moving boundary with different refractive indices across it. Past work has shown that such a moving boundary can reflect light in a dispersive medium, creating a forward-moving reflected wave with a significant frequency shift [9–12]. This effect is interpreted as a temporal analog of reflection of optical beams at a spatial boundary. Frequency of the reflected wave is set by a phase-continuity relation [13], which relies on both the dispersive nature of the material and the speed of the moving boundary.

In most previous studies, the boundary is assumed to move at a constant speed. However, when a pump pulse is used to create a moving temporal boundary through the optical Kerr effect [14,15], it is possible that the pulse's velocity itself changes with time. For short pump pulses propagating as solitons inside an optical fiber, the phenomenon of intrapulse Raman scattering provides a speed-changing mechanism by red-shifting the pump's spectrum in a continuous fashion. This phenomenon is referred to as the Raman-induced self-frequency shift (RIFS) [14,15]. As one would expect, the reflection process is significantly impacted when the boundary's speed changes during propagation [16]. In particular, the soliton can trap a dispersive wave through cascaded temporal reflections [17–19].

In this work, we use a photonic crystal fiber (PCF) as a nonlinear medium to study experimentally the temporal reflection of an optical pulse at a decelerating boundary, created by a short pump pulse undergoing the RIFS along the fiber's length. We find that the reflected pulse's spectrum changes significantly as the initial delay between the pump and probe pulses is varied. This process can be viewed as probing the trajectory of the decelerating temporal boundary. We show

#497251 https://doi.org/10.1364/OE.497251
Journal © 2023 Received 8 Jun 2023; revised 19 Jul 2023; accepted 24 Jul 2023; published 2 Aug 2023

Optics EXPRESS

that it is possible to deduce this trajectory from the delay-dependent spectral data. It should be stressed that the trajectory of a Raman soliton is hard to measure without destroying the fiber. Our approach provides a non-destructive method for deducing the soliton's trajectory. We believe that it can be used as a diagnostic tool for many other optical processes.

The paper is structured as follows. Section 2 introduces the basic concepts behind the temporal reflection of optical pulses at a moving boundary. We use numerical modeling in Section 3 to examine the reflection of a pulse from a short soliton undergoing the RIFS inside an optical fiber and discuss its important characteristics. In Section 4, we describe our experimental setup and analyze the data taken with it. We discuss and summarize our main results in Section 5.

2. Temporal reflection

It is well known that light reflected off a moving mirror undergoes a frequency shift relative to the incident light, known as the Doppler shift. However, when the moving "mirror" is formed in a dispersive medium, a different kind of reflection can occur. The physical process is depicted in Fig. 1(a). When light impinges upon a moving boundary that separates two dispersive media, it splits into reflected and transmitted parts. Unlike the standard Doppler effect, the reflected light continues to travel in the forward direction, but its speed changes with respect to the boundary to prevent it from crossing over. This change is achieved by shifting the frequency of reflected light and adjusting its speed as dictated by dispersion.

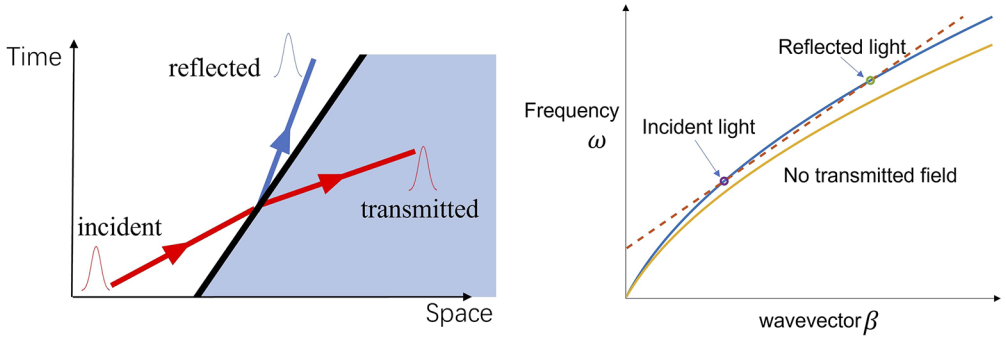

Fig. 1. (a) Schematic showing temporal reflection (blue line) of an incoming optical pulse (red line) from a moving boundary (thick black line) in a dispersive medium. (b) Phase-continuity relation (dashed line) in the β–ω space. The blue and yellow lines show the dispersion curves on the opposite sides of the moving boundary when the condition for total internal reflection is satisfied.

The phase-continuity relation [13] provides frequencies of the reflected and transmitted waves by ensuring that all three waves maintain a constant phase difference along the trajectory of the boundary. It can be expressed as:

$$\frac{\omega_r - \omega_i}{\beta_r - \beta_i} = \frac{\omega_t - \omega_i}{\beta_t - \beta_i} = v_b, \tag{1}$$

Here, ω_s and β_s with $s = i, r, t$ are the frequencies and wave vectors of the incident, reflected, transmitted waves respectively, while v_b is the speed of the boundary. Combining Eq. (1) with the dispersion relation of the material yields the frequencies of the reflected and transmitted light. This is illustrated in Fig. 1(b), where ω_s and β_s for the three waves are required to lie on the same straight line with a slope equal to the the boundary's speed (red dashed line). Dispersion of the medium enables this line to intersect the blue curve twice, resulting in a reflected wave as shown in Fig. 1(a). Remarkably, when the index difference is large enough across the boundary, this line

Optics EXPRESS

does not intersect the dispersion curve, and nothing is transmitted across the boundary. This phenomenon is the temporal analog of total internal reflection [9]. In optical fibers, such an effect has also been interpreted as optical analogue of the event horizon of a black hole [10,11].

The phase-continuity relation given in Eq. (1) establishes a clear dependence of the reflection-induced frequency shift on the speed of the boundary. If the boundary is not traveling at a constant speed, the reflected light will exhibit different frequency shifts depending on the time at which the incident light hits the moving boundary. This is illustrated in Fig. 2 using three pulses with different initial delays. Because the boundary's speed is changing as it propagates, central frequency of the reflected light depends on the relative delay between the incident pulse and the boundary. This feature allows us to deduce the boundary's trajectory through spectral measurements, effectively enabling us to probe this trajectory through temporal reflection.

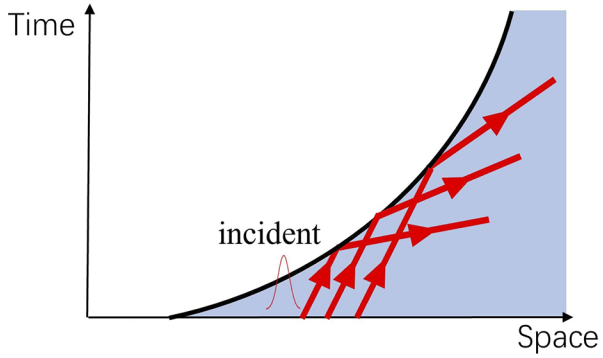

Fig. 2. Schematic showing temporal reflection of three probe pulses (red lines with arrows) from a decelerating boundary. Central frequency of the reflected pulse depends on the initial delay (or advance) of the probe pulse.

3. Modeling temporal reflection in an optical fiber

We employ a 3.8-m-long PCF (IXblue, IXF-SUP-2-135) for observing temporal reflection. A moving temporal region of higher refractive index is created by launching a short pump pulse in the anomalous-dispersion region of this fiber. The pulse forms a soliton and increases refractive index over its entire width through the optical Kerr effect. A probe pulse with its wavelength in the normal-dispersion region is also launched with a controllable delay.

The PCF used in our experiment was characterized by measuring its group delay with a technique based on white-light interferometry [20,21]. The results are shown in Fig. 3. The minimum delay occurs at the zero-dispersion frequency (406 THz) of the fiber. Pulses experience normal (anomalous) group-velocity dispersion when their central frequency is larger (smaller) than this frequency. We chose the pump's wavelength of 800 nm in the anomalous region so that it propagated as a soliton inside the PCF. The probe's wavelength was chosen in the normal region such that both pulses traveled with a small speed difference. As seen in Fig. 3, a probe pulse traveling slower than the soliton produces a reflected pulse moving faster than the soliton after its encounter with the soliton. By contrast, a probe pulse traveling faster than the soliton produces a reflected pulse moving slower than the soliton.

We simulate the reflection process numerically using two coupled nonlinear Schrodinger (NLS) equations governing evolution of the pump and probe pulses. The total electric field is written as

$$E(z,t_a) = \mathrm{Re}\left(A_s(z,t_a)e^{i[\beta(\omega_s)z-\omega_s t_a]} + A_p(z,t_a)e^{i[\beta(\omega_p)z-\omega_p t_a]}\right), \tag{2}$$

Optics EXPRESS

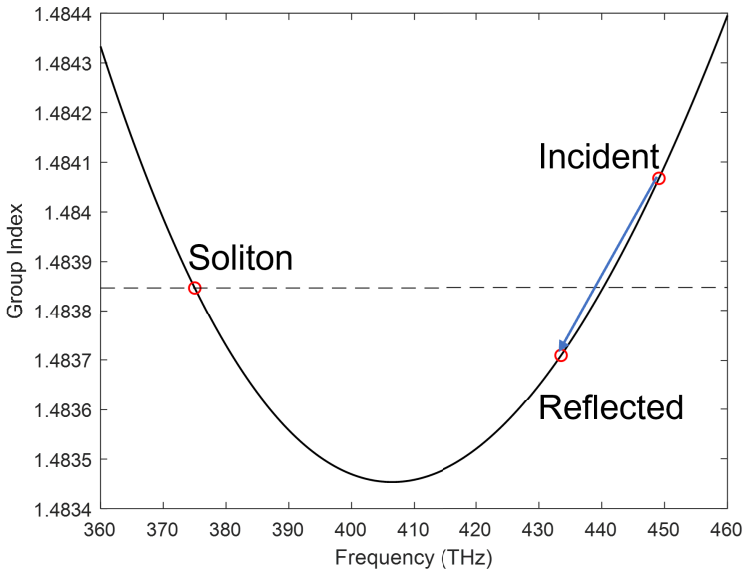

Fig. 3. Measured group index of the PCF plotted as a function of frequency. Its values for the soliton, incident probe pulse, and reflected pulse are marked by red circles.

where t_a is the time in the laboratory frame, ω_s and ω_p are the central frequencies, A_s and A_p are the envelopes of the soliton and probe pulse respectively, and $\beta(\omega)$ is the frequency-dependent propagation constant. Assuming that the probe energy is small enough that its nonlinear effects can be neglected, Maxwell's equations provide the following coupled NLS equations [14]:

$$\frac{\partial A_s}{\partial z} + \sum_{k\geq 2} \frac{i^{k-1}}{k!}\beta_k^{(s)} \frac{\partial^k A_s}{\partial t^k} = i\gamma \left(1 + \frac{i}{\omega_0}\frac{\partial}{\partial t}\right)\left((1-f_R)\,|A_s|^2 A_s + f_R N_R A_s\right), \tag{3}$$

$$\frac{\partial A_p}{\partial z} + \Delta\beta_1 \frac{\partial A_p}{\partial t} + \sum_{k\geq 2} \frac{i^{k-1}}{k!}\beta_k^{(p)} \frac{\partial^k A_p}{\partial t^k} = 2i\gamma |A_s|^2 A_p, \tag{4}$$

where $t = t_a - z/v_g(\omega_s)$ is the reduced time in a frame moving with the speed $v_g(\omega_s)$ and $\beta_k^{(j)} = (d^k\beta/d\omega^k)|_{\omega_j}$ with $j = s, p$ are the dispersion parameters of the PCF at the soliton and probe's frequencies respectively. The parameter, $\Delta\beta_1 = 1/v_g(\omega_p) - 1/v_g(\omega_s)$, is a measure of the speed difference between the probe and the soliton. As losses are <0.36 dB for our 3.8-m-long fiber (as per fiber's manufacturer), we have neglected the loss term in Eqs. (3) and (4).

For femtosecond pump pulses, it is important to include the effects of intrapulse Raman scattering governed by the nonlinear Raman term, $N_R = \int_0^\infty h_R(t')|A_s(z, t-t')|^2 dt'$, in Eq. (3), where $h_R(t)$ is the Raman response function. The parameter f_R sets the relative weight of the Raman contribution. We used the functional form of $h_R(t)$ with the f_R value given in Ref. [14]. The probe pulse is affected by the soliton through the cross-phase modulation term in Eq. (4).

We solved Eqs. (3) and (4) with the Runge–Kutta method using $A_s(0,t) = \sqrt{P_1}\mathrm{sech}(t/T_1)$ for the pump pulse with $T_1 = 15.7$ fs and $P_1 = |\beta_2^{(s)}|/(\gamma T_1^2)$ for the peak power of a fundamental soliton. The probe pulse was a much wider Gaussian pulse centered at 645 nm with a spectral width of 4 nm. The soliton had an initial delay of 1.15 ps relative to the probe pulse. The nonlinear coefficient for our PCF is estimated to be 105 $\mathrm{W^{-1}km^{-1}}$. In our experiments, we inject pump pulses with energy higher than that needed to form a fundamental soliton. After the fission process, a shorter Raman soliton is formed, whose spectrum shifts toward the red side with

Optics EXPRESS

propagation inside the fiber. For our numerical simulations, we use a short fundamental soliton to study probe's reflection from this Raman soliton. This is justified because only this Raman soliton has enough peak power to interact with the probe pulse.

Figure 4 shows our numerical results for the preceding parameter values. Temporal and spectral evolution patterns over the PCF length are shown for the (a) soliton (pump) and (b) probe pulse using a logarithmic color scale. Soliton trajectory would be vertical in the absence of the Raman effect. It appears nearly parabolic in part (a) because the soliton slows down because of its deceleration, owing to the RIFS or a continuous red-shift of the soliton's center frequency [14]. This red shift is seen clearly in the spectral evolution of the soliton in Fig. 4(a).

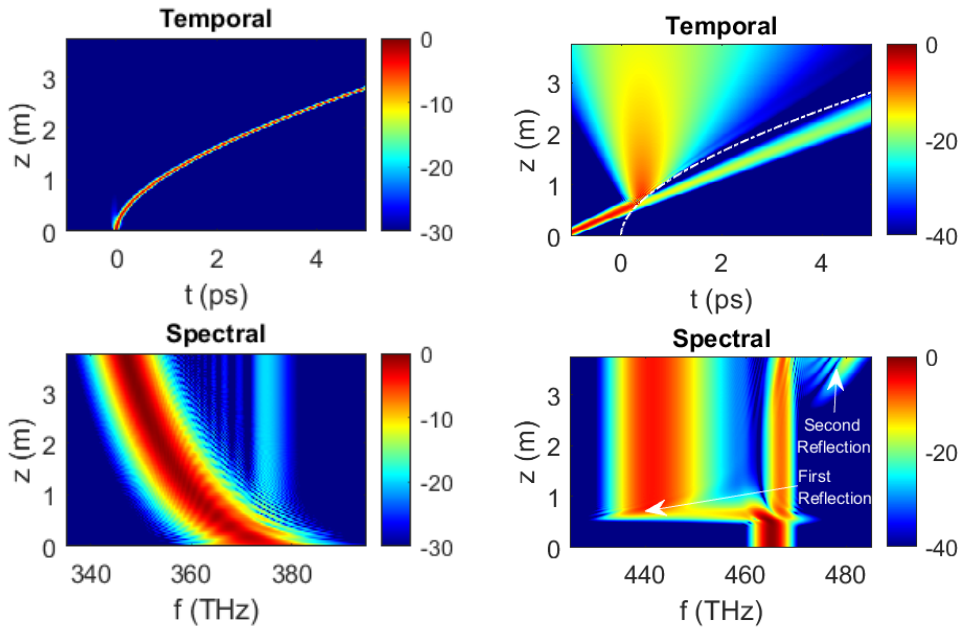

(a) Soliton (b) Probe pulse

Fig. 4. Temporal and spectral evolution patterns over the PCF length are shown for the (a) soliton (pump) and (b) probe pulse on a logarithmic color scale. The white dashed line in (b) shows trajectory of the soliton.

The probe pulse is initially traveling slower than the soliton. When the soliton collides with it, most of its energy gets reflected by the soliton. This is clearly seen from the probe's temporal evolution in Fig. 4(a). The reflected pulse travels faster than the soliton in the normal-dispersion region of the PCF because of a red shift in its spectrum. We can clearly identify this red-shifted peak in the spectral evolution of the probe (white arrow marked "first reflection"). However, a fraction of probe's energy is transmitted through the soliton, and this part keeps traveling slower than the soliton. As the soliton keeps decelerating inside the PCF, the transmitted part of the probe collides again with it, and a second reflected pulse is produced. This collision generates blue-shifted radiation near the end of the fiber (marked by the arrow "second reflection").

As discussed earlier, a change in the initial delay of the soliton from the probe pulse should change the spectrum of reflected pulse significantly. This is confirmed by performing simulations with different delays. The output spectra of the probe pulse with different delays are shown in Fig. 5. As the delay becomes larger, the probe's blue shift becomes smaller and eventually disappears. This can be understood from Fig. 2. As delay increases, speed difference between the probe and soliton decreases after they collide. When the delay is large enough, the soliton

Optics EXPRESS

does not catch up with the probe, and temporal reflection ceases to occur. The dashed black line in Fig. 5 is calculated by considering intersection of the probe's center with the soliton's decelerating trajectory. Frequency of the reflected pulse is calculated from Eq. (1) using v_b as the instantaneous speed of the soliton at that location (see supplemental for details). We find an excellent agreement between the simulated output spectrum and the analytical prediction of the central wavelength.

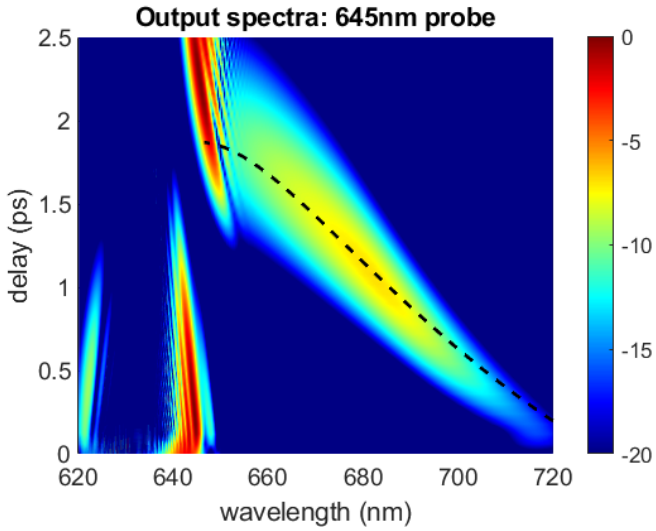

Fig. 5. Color-coded output spectrum of a 645-nm probe pulse for different initial delays between the pump and probe pulses.

Since the reflected pulse's spectrum depends on the speed of the soliton at the time of collision, we can deduce this speed by measuring the spectrum, which allows us to calculate the soliton's frequency. As we change the initial delay between the soliton and the probe, the probe pulse hits different parts of the trajectory of the soliton. Thus, the delay-dependent spectra shown in Fig. 5 contain information about the soliton's trajectory, making it possible to deduce the soliton's trajectory from the spectral data.

The soliton's spectrum shifts from 800 nm to 864 nm over the PCF length in Fig. 4(a). In this case, it is not possible to probe the whole trajectory using probe pulses at a single wavelength. The reason is that the efficiency of temporal reflection depends critically on the speed difference between the probe and the soliton [16]. As a result, probe pulses at one wavelength can only probe the portion of the soliton's trajectory where the speed difference is sufficiently small. To probe the whole trajectory, we send probe pulses at several different wavelengths. Combining the spectral data measured for different probe wavelengths, it became possible to probe the whole trajectory of the soliton.

4. Experimental results

In this section we focus on our pump-probe experiments performed with the setup shown in Fig. 6. A Ti:sapphire laser with a regenerative amplifier (Coherent, Astrella) emits pulses of about 30 fs duration with a spectrum centered at 800 nm. Half of the laser's output is sent into an optical parametric amplifier (Light Conversion, Opera-Solo), which generates pulses at tunable wavelengths. A band-pass filter (transmission spectrum has about 5 nm FWHM) provides probe pulses at a specific wavelength and limits their spectral bandwidth. The central wavelength of the

Optics EXPRESS

band-pass filter is tuned by tilting the filter at different angles. In this way, we were able to tune the central wavelength of the filter by about 30 nm.

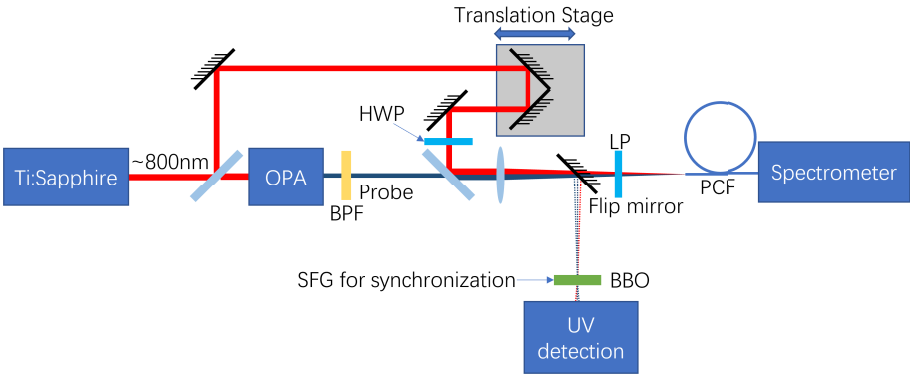

Fig. 6. Schematic of the experimental setup. OPA: optical parametric amplifier. BPF: band pass filter. HWP: half wave plate. LP: linear polarizer. PCF: photonic crystal fiber. SFG: sum-frequency generation

Pump pulses are sent through a translation stage before combining with probe pulses for precisely controlling the delay between them. Pump pulses are launched into the PCF with less than 10 pJ energy. Each pump pulse travels initially as a higher-order soliton whose fission generates a Raman soliton [14]. This Raman soliton acts as a moving boundary and reflects a probe pulse when the two pulses collide inside the fiber. A flip mirror determines whether to send the two pulses into the PCF or into a BBO for sum-frequency generation (SFG). The SFG signal is used to determine the zero-delay position of the soliton, defined as the position where the SFG is the largest. A linear polarizer is used before sending the pulses into the PCF to make sure that the pulses have polarization that aligns with one of the main axis of the PCF. The linear polarizer has dispersion, which causes the delay between the pump and probe to be different from the SFG result. Such discrepancy is eliminated by calculating this delay difference with the material's group index at different wavelengths. A half wave plate (HWP) is used to control the energy of the pump pulses launched into the PCF. The output of the PCF is measured by a spectrometer (Ocean Optics, USB2000).

We first consider the simpler case of temporal reflection without the Raman effect. This is achieved by carefully adjusting energy of the pump pulse sent into the fiber. By monitoring the output spectrum, it was possible to control energy such that a soliton is formed with negligible RIFS (at energy of about 2 pJ). Probe pulses at two different wavelengths (683 and 689 nm) are sent into the fiber, and the relative delay between the soliton and probe is tuned such that the whole probe pulse can reflect off the soliton, resulting in maximum reflectivity. We kept the energy of probe pulses relatively small to ensure that they do not impact pump pulses during propagation. For the results shown in Fig. 7, their energy was smaller than 0.03 pJ at 683 nm and 0.015 pJ at 689 nm. Probe pulses at these two wavelengths travel faster than the soliton. The input and output spectra of probe pulses are shown for comparison. After reflection, a blue shifted peak appears in the spectrum, which belongs to the reflected pulse traveling slower than the soliton. Comparing the probe pulses at the two wavelengths, the 689-nm probe has a larger initial speed difference, which makes the frequency shift of the reflected pulse larger with a smaller reflectivity. Using the incident and reflected probe spectra, we can calculate the soliton's wavelength at the time of collision from the phase-continuity relation in Eq. (1). The wavelength calculated this way is 802 nm, and this value is in agreement with the soliton's central wavelength seen in Fig. 7.

Optics EXPRESS

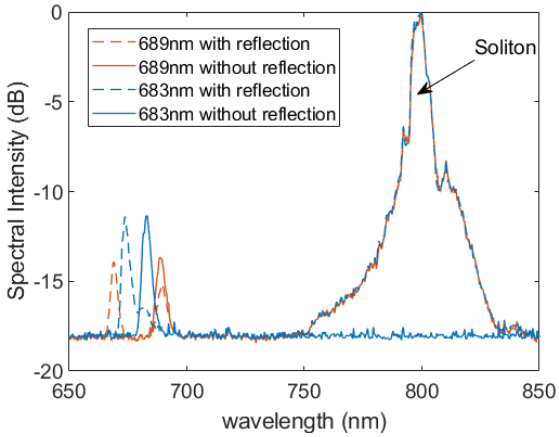

Fig. 7. Measured output spectra with three distinct peaks when the soliton undergoes negligible RIFS. Probe pulses at wavelengths 683 and 689 nm were reflected off the soliton formed by the 800-nm pump pulse. A blue-shifted reflected pulse (dashed line) is produced in both cases.

For the results shown in Fig. 8, the Raman effects were included by increasing energy of pump pulses launched into the PCF to about 7.4 pJ, which was large enough to form a higher-order soliton and create a short fundamental soliton through a fission process. The wavelength of this soliton shifts through RIFS toward the red side all along the PCF, resulting in a large shift at the output end. As seen in part (d) of Fig. 8, soliton's central wavelength has shifted from 800 to 864 nm over a length of just 3.8 m. Although some energy is left around 800 nm, it does not form another soliton and has a relatively minor impact on the probe pulse. We launched probe pulses at three wavelengths separated by 10 nm (645, 635 and 625 nm) and varied pump-probe delays to probe the soliton's trajectory. Theoretically, it has been shown that soliton's dynamics can be affected by energetic probe pulses [22]. We kept energy of probe pulses relatively small to ensure that the spectra of pump pulses were not affected by them. This energy in our experiment is estimated to be 0.2, 0.14, and 0.2 pJ at the wavelengths of 645, 635 and 625 nm, respectively. Measured output spectra as a function of pump-probe delay (positive delay means that pump arriving later than the probe) are shown for three probe wavelengths in parts (a), (b), and (c) of Fig. 8.

For probe wavelengths of 645 nm and 635 nm, we see a similar pattern. A red-shifted reflected pulse is formed after a specific delay, the red-shift becomes smaller as delay increases, and eventually becomes negligible when delay becomes relatively large. This trend is in good agreement with the simulations shown in Fig. 5. Notice that the maximum delay for which we can observe temporal reflection is different for different probe wavelengths. This is so because different probe wavelengths reflect off different portions of the soliton's trajectory.

When the probe's wavelength is 625 nm, the behavior is somewhat different. We still see a red-shifted peak with a decreasing red shift as delay increases. The difference is that this red-shifted peak does not merge with the original probe pulse's spectrum when delay becomes large. To understand this behavior, we note that probe pulses at wavelengths of 645 and 635 nm travel slower than the incident pump pulse, but faster than the output soliton. Thus, by changing the pump-probe delay, it is possible for the reflection to occur where the soliton and probe pulse have the same speed. On the space-time diagram shown in Fig. 2, the soliton and probe pulse's trajectory become parallel to each other. In this situation, reflected pulse's spectrum merges into the incident spectrum. In contrast, the 625-nm probe pulse travels slower than the output soliton all along the PCF length. As a result, their trajectories never becomes parallel. This is the reason

Optics EXPRESS

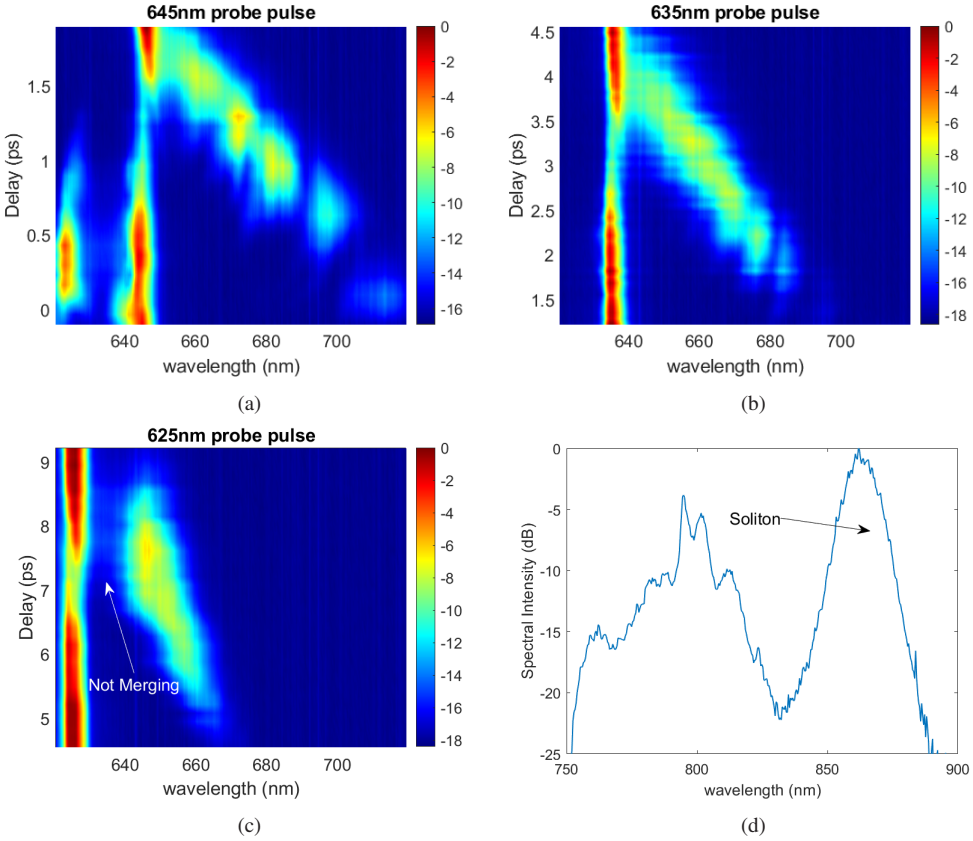

Fig. 8. Measured output spectra for different pump-probe delays when the incident probe's central wavelength was (a) 645 nm, (b) 635 nm and (c) 625 nm. Spectral intensity is shown in logarithmic scale relative to the probe's peak spectral intensity. (d) Output spectrum in the pump's spectral region.

why the reflected pulse's spectrum does not merge into the incident spectrum when the probe's wavelength is 625 nm.

As we discussed earlier, the delay-dependent spectra shown in Fig. 8 contain information about trajectory of the soliton inside the PCF. Here we briefly describe the approach we used for this purpose and refer to the Supplement for more details. The trajectory we want to extract specifies the soliton's wavelength (or speed) as a function of propagation distance. However, without knowing this trajectory, the location of pump-probe collision can not be determined for a given pump-probe delay. To solve this dilemma, we derive a differential equation, Eq.(S10), in the supplemental material using the phase-continuity relation in Eq. (1). This equation gave us a reasonable estimate of the trajectory. When we used this estimate in our simulations, we found that the predicted wavelengths did not agree well with the measured data. The reason is that the phase-continuity relation assumes reflection to occur at one location, while the probe pulses of finite duration interact with the pump over a range. We adjusted the trajectory estimated from phase-continuity relation with an iterative approach to obtain a better fit between the experimental data and numerical simulations.

The retrieved trajectory of the soliton's central wavelength is shown in part (d) of Fig. 9 with a red line; blue line shows trajectory of the soliton's central frequency. The space-time trajectory can be deduced from the spectral trajectory using the measured dispersion data of the PCF in

Optics EXPRESS

Fig. 3. We were not able to probe the trajectory over the first 0.5 m of the PCF, where the Raman soliton is produced through the fission process. A parabolic function was used in this region (see supplemental material for details). The shape of the the trajectory depends on the Raman-induced red shift occurring continuously all along the fiber. Interestingly, Fig. 9 shows that the rate of RIFS begins to saturate near the PCF's output end. This is because higher-order dispersive effects perturb the Raman soliton and force it to radiate some energy in the form of dispersive waves [14]. This trend can also be seen in the simulations shown in Fig. 4(a).

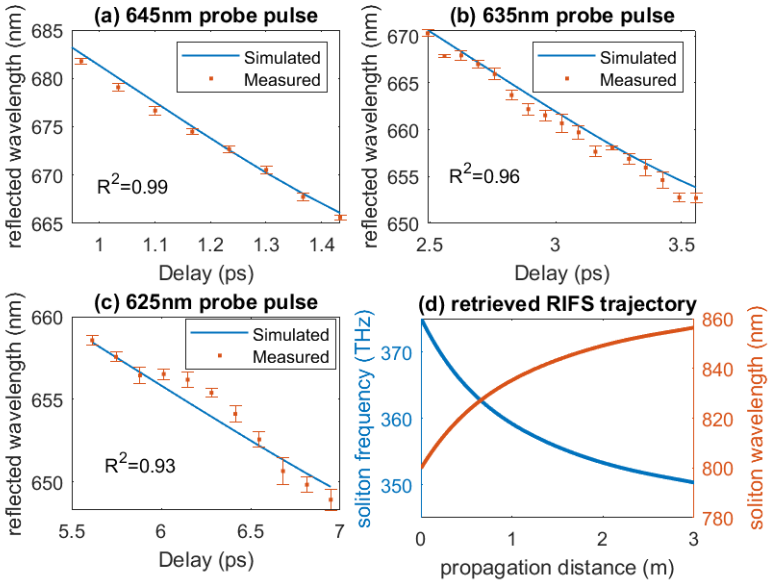

Fig. 9. (d) Retrieved trajectory of the soliton's wavelength based on the measured delay dependence of the reflected pulse spectra. Numerically predicted wavelength of the reflected pulse wavelength based on the retrieved trajectory for probe pulses launched at wavelengths (a) 645 nm, (b) 635 nm, and (c) 625 nm. Measured results are also shown for comparison.

To quantify how well the retrieved trajectory matches the actual soliton's trajectory, we performed simulations of the temporal reflection process for the three probe wavelengths (For details, see the supplement). We compare the numerical results with the measured data in parts (a), (b), and (c) of Fig. 9. The agreement is quantified by the R^2 values, $R^2 = 1$ indicating a perfect fit. As seen there, the agreement becomes worse for 625-nm probe pulses. The reason can be understood from part (c) of Fig. 8. As seen there, the red shift is much smaller at this wavelength and varies less rapidly with the delay, both of which make it harder to deduce the center wavelength of the reflected pulse accurately.

5. Discussion and conclusion

When a short pump pulse propagates as a soliton inside an optical fiber, it creates a moving high-index region through the optical Kerr effect. In this case, the phenomenon of intrapulse Raman scattering provides a speed-changing mechanism for the solitons by red-shifting the soliton's spectrum in a continuous fashion. If a probe pulse is launched into the same fiber with a delay such that it approaches the soliton at some location within the fiber, another pulse is generated through temporal reflection whose wavelength differs considerably from that the probe pulse. As one would expect, the process of temporal reflection and the spectral shift produced by it depend on the speed of the speed at that specific location. In this work, we propose and

Optics EXPRESS

demonstrate that the trajectory of the decelerating soliton can be probed using temporal reflection of probe pulses with different delays.

We used a photonic crystal fiber as a dispersive nonlinear medium to study experimentally the temporal reflection of probe pulses from a decelerating soliton undergoing the RIFS along the fiber's length. The 800-nm pump pulses formed short solitons because the PCF's group-velocity dispersion was anomalous at their wavelength. In contrast, probe pulses experienced normal dispersion when their wavelength was chosen to be shorter than the PCF's zero-dispersion wavelength (near 730 nm). Our experiments revealed that the wavelength of reflected probe pulses changed significantly when the initial pump-probe delay was varied. We used this feature to deduce the soliton's trajectory from the delay-dependent spectral data. Our approach provides a non-destructive method for analyzing how the soliton's speed is affected inside an optical fiber by the phenomenon of intrapulse Raman scattering.

Although we demonstrated the proposed technique for probing a soliton's trajectory, we believe that it can be used as a diagnostic tool for many other optical processes. For example, it may be possible to use a similar technique for probing the dispersive properties of a tapered waveguide. Tapering of a waveguide produces changes in its transverse size all along the length of the waveguide. When a short pulse is launched into a tapered waveguide such as an optical fiber, its speed changes along the fiber's length. Similar to the case of RIFS studied in this paper, reflected pulse's wavelength would depend on the dispersive properties of the fiber at the location where the pump and prove pulses collide. The tapering approach is more versatile than the RIFS studied here because one has more control on the nature and magnitude of speed changes. It should also be possible to use the proposed technique as a diagnostic tool for the process of supercontinuum generation by launching a probe pulse with the pump pulse and controlling their relative time delay.

Funding. National Science Foundation (ECCS-1933328); U.S. Department of Energy (DE-NA0003856).

Acknowledgement. This work is supported by National Science Foundation (ECCS-1933328).

This material is based upon work supported by the Department of Energy National Nuclear Security Administration under Award Number DE-NA0003856, the University of Rochester, and the New York State Energy Research and Development Authority.

Disclosures. The authors declare no conflicts of interest.

Data Availability. Data underlying the results presented in this paper are not publicly available at this time but may be obtained from the authors upon reasonable request.

Supplemental document. See Supplement 1 for supporting content.

References

1. E. Galiffi, R. Tirole, S. Yin, H. Li, S. Vezzoli, P. A. Huidobro, M. G. Silveirinha, R. Sapienza, A. Alù, and J. Pendry, "Photonics of time-varying media," Adv. Photonics **4**(01), 014002 (2022).
2. C. Caloz and Z.-L. Deck-Léger, "Spacetime metamaterials-part I: general concepts," IEEE Trans. Antennas Propag. **68**(3), 1569–1582 (2020).
3. C. Caloz and Z.-L. Deck-Leger, "Spacetime metamaterials-part II: theory and applications," IEEE Trans. Antennas Propag. **68**(3), 1583–1598 (2020).
4. F. Miyamaru, C. Mizuo, T. Nakanishi, Y. Nakata, K. Hasebe, S. Nagase, Y. Matsubara, Y. Goto, J. Pérez-Urquizo, J. Madéo, and K. Dani, "Ultrafast frequency-shift dynamics at temporal boundary induced by structural-dispersion switching of waveguides," Phys. Rev. Lett. **127**(5), 053902 (2021).
5. Y. Xiao, D. N. Maywar, and G. P. Agrawal, "Reflection and transmission of electromagnetic waves at a temporal boundary," Opt. Lett. **39**(3), 574–577 (2014).

Optics EXPRESS

6. R. Tirole, S. Vezzoli, E. Galiffi, I. Robertson, D. Maurice, B. Tilmann, S. A. Maier, J. B. Pendry, and R. Sapienza, "Double-slit time diffraction at optical frequencies," Nat. Phys. **19**(7), 999–1002 (2023).
7. X. Wang, M. S. Mirmoosa, V. S. Asadchy, C. Rockstuhl, S. Fan, and S. A Tretyakov, "Metasurface-based realization of photonic time crystals," Sci. Adv. **9**(14), eadg7541 (2023).
8. Y. Sharabi, A. Dikopoltsev, E. Lustig, Y. Lumer, and M. Segev, "Spatiotemporal photonic crystals," Optica **9**(6), 585–592 (2022).
9. B. W. Plansinis, W. R. Donaldson, and G. P. Agrawal, "What is the temporal analog of reflection and refraction of optical beams?" Phys. Rev. Lett. **115**(18), 183901 (2015).
10. T. G. Philbin, C. Kuklewicz, S. Robertson, S. Hill, F. Konig, and U. Leonhardt, "Fiber-optical analog of the event horizon," Science **319**(5868), 1367–1370 (2008).
11. K. E. Webb, M. Erkintalo, Y. Xu, N. G. Broderick, J. M. Dudley, G. Genty, and S. G. Murdoch, "Nonlinear optics of fibre event horizons," Nat. Commun. **5**(1), 4969 (2014).
12. L. Tartara, "Frequency shifting of femtosecond pulses by reflection at solitons," IEEE J. Quantum Electron. **48**(11), 1439–1442 (2012).
13. M. A. Gaafar, T. Baba, M. Eich, and A. Y. Petrov, "Front-induced transitions," Nat. Photonics **13**(11), 737–748 (2019).
14. G. P. Agrawal, *Nonlinear fiber optics*, (Academic Press, 2019), 6th ed.
15. S. Robertson and U. Leonhardt, "Frequency shifting at fiber-optical event horizons: the effect of Raman deceleration," Phys. Rev. A **81**(6), 063835 (2010).
16. J. Zhang, W. Donaldson, and G. P. Agrawal, "Temporal reflection of an optical pulse from a short soliton: impact of Raman scattering," J. Opt. Soc. Am. B **39**(7), 1950–1957 (2022).
17. A. V. Gorbach and D. V. Skryabin, "Light trapping in gravity-like potentials and expansion of supercontinuum spectra in photonic-crystal fibres," Nat. Photonics **1**(11), 653–657 (2007).
18. D. R. Austin, C. M. de Sterke, B. J. Eggleton, and T. G. Brown, "Dispersive wave blue-shift in supercontinuum generation," Opt. Express **14**(25), 11997–12007 (2006).
19. N. Nishizawa and T. Goto, "Pulse trapping by ultrashort soliton pulses in optical fibers across zero-dispersion wavelength," Opt. Lett. **27**(3), 152–154 (2002).
20. P. Hlubina, M. Szpulak, D. Ciprian, T. Martynkien, and W. Urbańczyk, "Measurement of the group dispersion of the fundamental mode of holey fiber by white-light spectral interferometry," Opt. Express **15**(18), 11073–11081 (2007).
21. T. Kardaś and C. Radzewicz, "Broadband near-infrared fibers dispersion measurement using white-light spectral interferometry," Opt. Commun. **282**(22), 4361–4365 (2009).
22. A. Demircan, S. Amiranashvili, and G. Steinmeyer, "Controlling light by light with an optical event horizon," Phys. Rev. Lett. **106**(16), 163901 (2011).